High-precision joint estimation of the state of charge and state of energy for new energy electric vehicle lithium-ion batteries based on improved singular value decomposition-adaptive embedded cubature Kalman filtering.

ZHOU, J., WANG, S., CAO, W., XIE, Y. and FERNANDEZ, C.

2023

High-precision joint estimation of the state of charge and state of energy for new energy electric vehicle lithium-ion batteries based on improved singular value decomposition-adaptive embedded cubature Kalman filtering

Jiani Zhou[1] Shunli Wang[1,2*] Wen Cao[1] Yanxin Xie[1] Carlos Fernandez[3]

1. **School of Information Engineering, Southwest University of Science and Technology, Mianyang 621010, China**
2. **School of Electrical Engineering, Sichuan University, Chengdu 610065, China**
3. **School of Pharmacy and Life Sciences, Robert Gordon University, Aberdeen AB10-7GJ, UK**

*** Corresponding author: Shunli Wang 497420789@qq.com**

Abstract

Accurate online estimation of the state of charge (SOC) and state of energy (SOE) of lithium-ion batteries are essential for efficient and reliable energy management of new energy electric vehicles (EVs). To improve the accuracy and stability of the joint estimation of SOC and SOE of lithium-ion batteries for EVs, based on a dual-polarization (DP) equivalent circuit model and time-varying forgetting factor recursive least squares (TVFFRLS) algorithm for online parameter identification, a joint estimation method based on singular value decomposition with adaptive embedded cubature Kalman filtering (SVD-AECKF) algorithm is proposed. The algorithm adopts the embedded cubature criterion and singular value decomposition method to improve filtering efficiency, accuracy, and numerical stability. Meanwhile, combining the idea of adaptive covariance matching for real-time adaptive updating of system noise to improve joint estimation accuracy. Finally, the results under different initial errors and complex operating conditions show that the SVD-AECKF algorithm improves the convergence time of SOC estimation by at least 26.3% compared to that before optimization. The SOE estimation error is reduced by at least 12.0% compared to that before optimization. This indicates that the SVD-AECKF algorithm has good joint SOC and SOE estimation accuracy, convergence, and stability.

Keywords Lithium-ion batteries · State of charge · State of energy · Adaptive embedded cubature Kalman filtering · Time- varying forgetting factor · Singular value decomposition

Introduction

The new energy storage system becomes a key means for advancing clean energy, the energy revolution, and the development of sustainable energy under the direction of the "double carbon" strategy [1]. In the new energy storage system, lithium-ion batteries (LIBs) have been widely used in new energy electric vehicles as the "power source" of electric vehicles due to their high energy density, long cycle life, and low self-discharge rate [2, 3]. It directly affects the driving range, vehicle quality, and manufacturing cost, and has been a key factor limiting the development of electric vehicles [4, 5]. Battery performance is affected by operating conditions and battery status [6]. However, numerous factors influence the lifetime of LIBs [7]. Overcharging or over-discharging will speed up the aging of the battery and lead to changes in the service life of the battery. In serious cases, it is easy to cause battery fire and explosion, and it greatly reduces the safety of new energy electric vehicles [8–11]. Thus, it is particularly important to use a battery management system (BMS) to enable the monitoring and control of LIBs in electric vehicles.

The SOC estimation of LIBs is one of the important functions of BMS. It not only indicates the remaining power of the battery but also manages and controls the charging and discharging processes of the battery in a balanced manner, ensuring the stable operation of the power battery [12]. The battery SOC estimation value is difficult to measure, and it is affected by a variety of factors such as voltage, charge/ discharge multiplier, working environment temperature, etc. [13]. As a result, it can only be obtained indirectly through other physical quantities and algorithms. The ampere-time integration method, open-circuit voltage method, internal resistance analysis method, data-driven algorithm, and model-based algorithm are the major methods used by both local and international academics to estimate battery charge state at the moment [14, 15].

Among them, the open-circuit voltage method, the ampere-time integration method, and the internal resistance analysis method are the three early traditional methods [16]. C. Huang et al. [17] applied the open-circuit voltage method as an initial value correction for the Ah integration method to estimate the battery SOC and found that the open-circuit voltage leads to large deviations in SOC at different temperatures. The data-driven algorithms mainly include neural networks (NN), support vector machines (SVM), fuzzy logic (FL), and other intelligent computing methods [18]. This intelligent computing method is highly complex and requires a large number of data samples to train the battery model, which can easily lead to random output results and possibly large errors [19]. Compared with traditional methods and data-driven class algorithm methods, model-based algorithms for SOC estimation are more commonly used today [20]. The main methods in this category are Kalman filtering methods, particle filtering methods, and H∞ filtering methods, as well as other improved fusion algorithms [21–23]. The estimation of electrical SOC using a Kalman filter requires an accurate battery model, and the model and parameters are different for different types of batteries [24–26]. To better exploit the charging and discharging characteristics of the LIBs and reduce the impact of overcharge and over-discharge on the cycle life of the LIBs, Shiqiang Zhuang et al. [27] proposed the cubature Kalman filter (CKF) algorithm to estimate the SOC. Experimental results show that the maximum error of the algorithm to estimate the SOC is kept within 4% and the average error is kept within 1%. However, there are problems that it is difficult to accurately obtain the statistical characteristics of the measurement noise and there is the possibility of losing the positive characteristics in the iterative process leading to the reduction of the filtering accuracy [28–32]. Therefore, continuous optimization of the algorithm is required to effectively improve the battery state estimation. SOE is one of the basic parameters of the battery safety protection module in BMS, which directly reflects the internal energy change of the battery [33]. Under the current situation where the range estimation accuracy is not high, SOE is used to achieve the range estimation of new energy vehicles and provide the driver with accurate range information [34–36]. Accurate SOE estimation not only helps the battery management system to develop a reasonable energy control strategy and optimize the energy control performance of new energy electric vehicles but also has practical significance to promote the development and promotion of electric vehicles [37–41]. The classification of the SOE estimation method is roughly the same as that of the SOC estimation method, which can be divided into the direct method, model-based method, and data-driven method [42–44]. The power integration method is one of the direct methods, which has the advantages of rapidity and high efficiency, but it also has the disadvantage of being susceptible to environmental disturbances leading to accuracy degradation. Xin Lai et al. [34] proposed a joint method using a particle filter (PF) and extended Kalman filter (EKF) for high-precision estimation of SOE, with a maximum estimation error of less than 3%. Zhang et al. [45] used a model-driven method with an adaptive traceless Kalman filter to achieve an adaptive noise covariance matrix in the calculation process, which further improved the accuracy and achieved SOE accurate estimation. L. Ma et al. [38] proposed a data-driven method for simultaneous estimation of SOC and SOE based on long short-term memory (LSTM) deep neural network and verified the effectiveness of the algorithm by two dynamic drive cycles under different operating conditions such as different temperatures, different battery materials, and noise interference. Xiao Yang et al. [44] used two modular adaptive controllers to optimize the CKF algorithm for joint estimation of SOC and SOE in lithium-ion batteries. Under complex conditions, the experimental results show that the rate of convergence of SOC estimation is improved by 52.17%, and the maximum error of SOE estimation is 0.0463, which is 24.59% less than that of the traditional CKF algorithm. The algorithm significantly improves the joint estimation accuracy and rate of convergence. However, the method selects a fixed value for the cubature point weights, and this can easily lead to the selected cubature points exceeding the integration region and making the algorithm unworkable.

To improve the accuracy and stability of battery state estimation in the complex operating environment of the LIBs in new energy electric vehicles, an improved SVD-AECKF algorithm for joint online high accuracy estimation is proposed in this article. The main contributions of this article are as follows.

(1) The TVFFRLS algorithm can improve the accuracy of DP equivalent circuit model parameter identification by changing the forgetting factor in real time.

(2) The proposed SVD-AECKF algorithm not only uses the embedded cubature criterion and singular value decomposition (SVD) method to improve the filtering accuracy, efficiency, and numerical stability but also combines the idea of adaptive covariance matching to reduce the influence of system noise on the estimation in complex environments, thus extending the applicability of the algorithm and improving the joint estimation accuracy.

(3) The CKF algorithm, embedded cubature Kalman filtering (ECKF) algorithm, and singular value decomposition-embedded cubature Kalman filtering (SVD-ECKF) algorithm are experimentally validated against the SVD-AECKF algorithm under different operating conditions, and the convergence speed, maximum error, and average error factors are compared. The experimental results show that the proposed SVD-AECKF algorithm has the best convergence and the highest accuracy in the joint estimation of SOC and SOE.

Mathematical analysis

Double polarization equivalent circuit model

In consideration of model complexity and accuracy, this article proposes to use the equivalent circuit model for battery state estimation. The typical equivalent models commonly used at home and abroad are the internal resistance (Rint) model, the partnership for the new generation of vehicles (PNGV) model, the Thevenin circuit model, the multi-order RC model, etc. The structure of the Rint model is very simple, and the model has only one ohmic internal resistance, which cannot well represent the battery transient response process and internal polarization phenomena, and cannot be used as the basis of the joint estimation research. The Thevenin model adds an RC parallel circuit to the Rint model, which fully takes into account the polarization characteristics of the LIBs and can describe the polarization phenomenon of batteries more completely. The PNGV model is based on the Thevenin model with the addition of a series capacitor, which makes up for the disadvantage of the constant open circuit voltage of the Thevenin circuit model. However, the PNGV model is relatively complicated in parameter identification and not easy to implement. Combining the accuracy, complexity, and implementation analysis of the model, this article proposes to use the dual-polarization (DP) equivalent model to model the LIBs, and the circuit schematic is shown in Fig. 1.

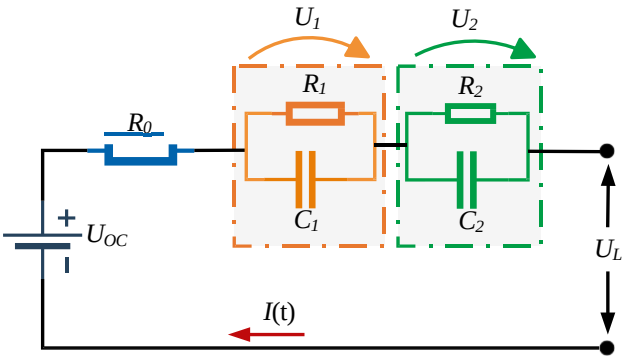

Fig. 1 DP equivalent circuit model

The DP equivalent model is based on the Thevenin model and uses a series of resistive capacitive parallel circuits. It not only accurately reflects the polarization effect of LIBs but also facilitates LIB characterization and parameter identification. Based on Kirchhoff's voltage law, the state expressions of voltage and current are obtained by analyzing the circuit as shown in Eq. (1).

$$\begin{cases} U_L = U_{oc} - I(t)R_0 - U_1 - U_2 \\ \frac{dU_1}{dt} = -\frac{U_1}{R_1C_1} + \frac{I}{C_1} \\ \frac{dU_2}{dt} = -\frac{U_2}{R_2C_2} + \frac{I}{C_2} \end{cases} \tag{1}$$

In Eq. (1), U_{OC} denotes the open circuit voltage of the battery; U_L is the terminal voltage of the battery; I is the operating current of the battery; C and R denote the resist- ance and capacitance of the battery.

Combining the SOC and SOE definition equations, choose to select $[SOC\ U_1\ U_2]^T$ and $[SOE\ U_1\ U_2]^T$ are chosen as the state variables of SOC and SOE, respectively. Then the equivalent circuit model is discretized, and the discrete state space square expressions can be obtained as shown in Eqs. (2) and (3).

$$\begin{cases} SOC(t) = SOC(t_0) - \eta \int_{t_0}^{t} \frac{I}{Q_N} dt \\ \begin{bmatrix} SOC_{k+1} \\ U_{1,k+1} \\ U_{2,k+1} \end{bmatrix} = \begin{bmatrix} 1 & 0 & 0 \\ 0 & e^{-\frac{\Delta t}{\tau_1}} & 0 \\ 0 & 0 & e^{-\frac{\Delta t}{\tau_2}} \end{bmatrix} \begin{bmatrix} SOC_k \\ U_{1,k} \\ U_{2,k} \end{bmatrix} + \begin{bmatrix} -\frac{\eta \Delta t}{Q_N} \\ R_1\left(1 - e^{-\frac{\Delta t}{\tau_1}}\right) \\ R_2\left(1 - e^{-\frac{\Delta t}{\tau_2}}\right) \end{bmatrix} I_k + w_{k1} \\ U_{L1,k+1} = U_{oc(SOC,k+1)} - U_1 - U_2 - IR_0 + v_{k1} \end{cases} \tag{2}$$

$$\begin{cases} SOE(t) = SOE(t_0) - \eta \int_{t_0}^{t} \frac{U_L I}{E_N} dt \\ \begin{bmatrix} SOE_{k+1} \\ U_{1,k+1} \\ U_{2,k+1} \end{bmatrix} = \begin{bmatrix} 1 & 0 & 0 \\ 0 & e^{-\frac{\Delta t}{\tau_1}} & 0 \\ 0 & 0 & e^{-\frac{\Delta t}{\tau_2}} \end{bmatrix} \begin{bmatrix} SOE_k \\ U_{1,k} \\ U_{2,k} \end{bmatrix} + \begin{bmatrix} -\frac{\eta U_{L,k} \Delta t}{E_N} \\ R_1\left(1 - e^{-\frac{\Delta t}{\tau_1}}\right) \\ R_2\left(1 - e^{-\frac{\Delta t}{\tau_2}}\right) \end{bmatrix} I_k + w_{k2} \\ U_{L2,k+1} = U_{oc(SOE,k+1)} - U_1 - U_2 - IR_0 + v_{k2} \end{cases} \tag{3}$$

In Eqs. (2) and (3), Δt is the sampling interval; is the time constant, $r = RC$ is the time constant of the electrochemical circuit; w_k is the state noise; and v_k is the measurement noise, which is the zero-mean white noise of the covariance matrices Q and R, respectively; Q_N is the rated capacity of the battery; E_N is the total energy of the battery; r, is the charging and discharging efficiency of the LIBs, which is set to 0.98.

Online parameter identification based on TVFFRLS

The recursive least squares (RLS) algorithm based on the theory of minimizing the sum of squares of errors is a commonly used system parameter optimization identification technique. The algorithm is simple in principle and easy to implement, and is widely used for online identification of model parameters of the LIBs. With the increase of observed data, new data is easy to be submerged by old data, and the phenomenon of "data saturation" occurs; thus, the RLS algorithm cannot accurately track the changes in model parameters in real time. The least squares algorithm with fixed forgetting factor (FFRLS) reduces the proportion of old data information in the gain and reduces the impact of data saturation by adding a fixed forgetting factor. The core formula is shown in Eq. (4).

$$\begin{cases} e_k = y_k - \varphi_k^T \hat{\theta}_{k-1} \\ \hat{\theta}_k = \hat{\theta}_{k-1} + K_k e_k \\ K_k = \frac{P_{k-1} \varphi_k^T}{\varphi_k^T P_{k-1} \varphi_{k+} \lambda_k} \\ P_k = \frac{1}{\lambda_k}(1 - K_k \varphi_k^T) P_{k-1} \end{cases} \tag{4}$$

In Eq. (4), y_k is the output of the system; rp_k is the input of the system; e_k is the prediction error of the terminal voltage; Kk is the algorithm gain matrix; 0,..k is the parameter variable. Due to the LIBs of new energy electric vehicles usually working in a complex time-varying environment, the rapidly changing current will lead to large errors in the identification results of the FFRLS algorithm with a fixed forgetting factor, and it cannot meet the requirements of identification accuracy. Therefore, based on the FFRLS algorithm, an improved time-varying forgetting factor recursive least squares (TVFFRLS) algorithm is formed by automatically finding the optimal value of the forgetting factor by the voltage mean square error at data points within the data sliding window in different time-varying environments to improve the stability and recognition accuracy of online parameter tracking. This time-varying forgetting factor λ of the algorithm is calculated following Eq. (5):

$$\begin{cases} \lambda_k = \lambda_{\min} + e^{L_k}(\lambda_{\max} - \lambda_{\min}) \\ L_k = -\rho \frac{\sum_{i=k-M+1}^{k} e_i e_i^T}{M} \end{cases} \tag{5}$$

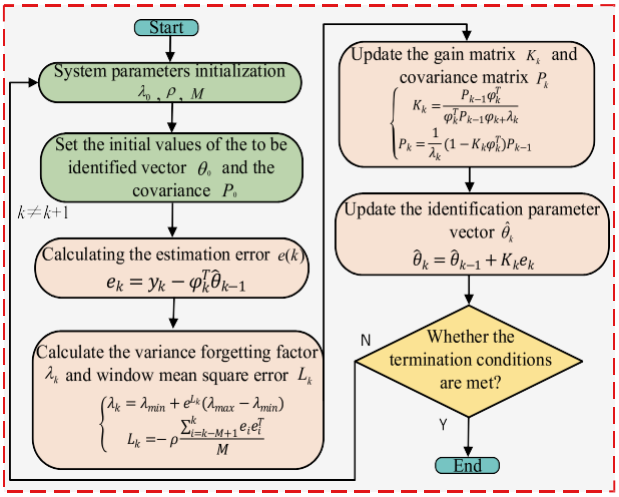

Fig. 2 Flow block diagram of TVFFRLS algorithm

In Eq. (5), k represents the current data point; λ_k is the forgetting factor obtained from the current operation; $\lambda_{\max}$ and $\lambda_{\min}$ are the maximum and minimum values of the forgetting factor, respectively; M is the window size; e_i is the terminal voltage error at the ith data point. p is the sensitivity factor; L_k is the mean squared error of the voltage at the kth data point. The flow chart of the process of parameter identification by the TVFFRLS algorithm is shown in Fig. 2

Improved AECKF algorithm based on the SVD method

The cubature Kalman filtering (CKF) algorithm is a nonlinear filtering algorithm. Compared with other nonlinear Kalman filtering algorithms, it has the features of good filtering effect, scalability, and less time consumption. The traditional CKF algorithm uses a third-order spherical mirror cubature criterion to select a fixed value of cubature point weights. It can easily cause the selected cubature points to exceed the integration region and make the algorithm inoperable. Therefore, to address the shortcomings of the CKF algorithm, this paper proposed an embedded cubature Kalman filter (ECKF) algorithm by using the embedded cubature criterion instead of the spherical mirror cubature criterion.

The embedded cubature criterion changes the number of cubature points of the n-order system from $2n$ to $2^n + 1$. It not only expands the integration range of cubature points and solves the problem of fixing the corresponding weights of cubature points but also avoids the inherent defects of the spherical-radial cubature criterion and improves the efficiency and accuracy of the algorithm. The rules for finding the set of cubature points ζ_i and the corresponding weights w_i of the CKF algorithm under the embedded cubature criterion are as follows in Eqs. (6) and (7).

$$\zeta_i = \begin{cases} [0]_i, i = 1 \\ \sqrt{2}[\delta]_i, i = 2, \cdots, 2^n + 1 \end{cases} \tag{6}$$

$$\omega_i = \begin{cases} 1 - \frac{1}{2u^2}, i = 1 \\ \frac{1}{2^{n+1}u^2}, i = 2, \cdots, 2^n + 1 \end{cases} \tag{7}$$

In Eqs. (6) and (7), $[\delta]_i$ is the i-th cubature point; δ is a free parameter, and δ is empirically taken to a value of 1 in this study; is the embedded family parameter, generally taken as 1; n is the state dimension.

As the number of algorithm iterations increases, the gradual increase in data error can easily lead to the loss of the positivity and symmetry of the state covariance matrix. The Cholesky decomposition in the a priori estimated covariance can easily lead to filtering interruptions and reduce the stability of the algorithm. Therefore, this paper proposes to introduce the singular value decomposition (SVD) matrix method to replace the traditional Cholesky decomposition method to improve the stability and performance of numerical computation. Take a matrix P of order $m \times n$ as an example; it can be decomposed into the following Eq. (8) form by SVD:

$$\begin{cases} P = U\begin{bmatrix} S & 0 \\ 0 & 0 \end{bmatrix} V^T \\ S_P = U\sqrt{S} \end{cases} \tag{8}$$

In Eq. (8), matrix U and matrix V are unitary matrices of order m and order n, respectively; S matrix is a diagonal matrix consisting of singular values of P.

Combining the embedded cubature criterion and cubature Kalman filter theory, the specific implementation steps of the joint estimation of SOC and SOE for lithium-ion batteries using the matrix decomposition method of SVD are shown below.

Step 1 Initialization

1.1 Initialize the posterior error covariance P_0

1.2 Initialize the state vector x_0

1.3 Initialize the process noise covariance Q_0.

1.4 Initialize the measurement noise covariance R_0.

1.5 Calculate the initial mean $'''x_0$ and covariance P_0 with a randomly selected state vector x_0:

$$\begin{cases} \hat{x}_0 = E(x_0) \\ P_0 = E\left[(\hat{x}_0 - x_0)(\hat{x}_0 - x_0)^T\right] \end{cases} \tag{9}$$

Step 2 Update of time

2.1 Perform SVD decomposition of the initial variance

$$P_{\frac{k-1}{k-1}} = U_{k-1}\sqrt{S_{k-1}}V_{k-1}^T \tag{10}$$

2.2 Calculate the cubature point according to the embedded cubature criterion:

$$\begin{cases} x_{i,\frac{k-1}{k-1}} = U_{k-1}\sqrt{S_{k-1}}\xi_i + \hat{x}_{\frac{k-1}{k-1}} \\ \zeta_i = \begin{cases} [0]_i, i = 1 \\ \sqrt{2}[\delta]_i, i = 2, \cdots, 2^n + 1 \end{cases} \\ \omega_i = \begin{cases} 1 - \frac{1}{2\delta^2}, i = 1 \\ \frac{1}{2^{n+1}\delta^2}, i = 2, \cdots, 2^n + 1 \end{cases} \end{cases} \tag{11}$$

$_i$

2.3 Propagation of cubature points through the equation of state:

$$x^*_{i,\frac{k}{k-1}} = f\left(x_{\frac{k-1}{k-1}}, u_k\right), i = 1, 2, \cdots m \tag{12}$$

2.4 Calculate the predicted state:

$$\hat{x}_{\frac{k}{k-1}} = \sum_{i=1}^{m} \omega_i x^*_{i,\frac{k}{k-1}} \tag{13}$$

2.5 Calculate the propagated covariance:

$$P_{\frac{k}{k-1}} = \frac{1}{m} \sum_{i=1}^{m} x^*_{i,\frac{k}{k-1}} x^{*T}_{i,\frac{k-1}{k-1}} - \hat{x}_{\frac{k}{k-1}}\hat{x}^T_{i,\frac{k}{k-1}} + Q_{k-1} \tag{14}$$

Step 3 Update of measurement

3.1 Covariance matrix SVD transformation and recalculation of the cubature points:

$$\begin{cases} P_{\frac{k}{k-1}} = U_{K-1}^{*}\sqrt{S_{k-1}^{*}}V_{k-1}^{*T} \\ x_{i,\frac{k}{k-1}} = U_{K-1}^{*}\sqrt{S_{k-1}^{*}}\xi_i + \hat{x}_{\frac{k}{k-1}} \end{cases} \tag{15}$$

3.2 Propagate the cubature points and calculate the predicted measurement:

$$\begin{cases} y_{i,\frac{k}{k-1}}^{*} = h\left(x_{i,\frac{k}{k-1}}, u_k\right), i = 1, 2, \cdots m \\ \hat{y}_{\frac{k}{k-1}} = \sum_{i=1}^{m} \omega_i y_{i,\frac{k}{k-1}}^{*} \end{cases} \tag{16}$$

Step 3.3 Calculate the predicted values of the measurements:

$$\hat{y}_{\frac{k}{k-1}} = \sum_{i=1}^{m} \omega_i y_{i,\frac{k}{k-1}}^{*} \tag{17}$$

Step 3.4 Calculate the error covariance matrix and the cross-covariance matrix:

$$\begin{cases} P_{yy,\frac{k}{k-1}}^{SOX} = \frac{1}{m}\sum_{i=1}^{m} \omega_i (y_{i,\frac{k}{k-1}}^{*} - \hat{y}_{\frac{k}{k-1}})\left(y_{i,\frac{k}{k-1}}^{*} - \hat{y}_{\frac{k}{k-1}}\right)^{T} + R_{k-1} \\ P_{xy,\frac{k}{k-1}} = \frac{1}{m}\sum_{i=1}^{m} \omega_i \left(x_{i,\frac{k}{k-1}} - \hat{x}_{i,\frac{k}{k-1}}\right)\left(y_{i,\frac{k}{k-1}}^{*} - \hat{y}_{i,\frac{k}{k-1}}\right)^{T} + R_{k-1} \end{cases} \tag{18}$$

where *SOX* represents the estimated state of the battery

Step 4 Update of the system state

Step 4.1 Calculate the Kalman gain:

$$K_k = P_{xy,\frac{k}{k-1}}(P_{yy,\frac{k}{k-1}}^{SOX})^{-1} \tag{19}$$

Step 4.2 Update the posterior state:

$$\hat{x}_{SOX,\frac{k}{k}} = \hat{x}_{\frac{k}{k-1}} + K_k(y_k - \hat{y}_{\frac{k}{k-1}}) \tag{20}$$

Step 4.3 Update the error covariance matrix:

$$P_{\frac{k}{k}} = P_{\frac{k}{k-1}} - K_k P_{yy,\frac{k}{k-1}} K_k^{T} \tag{21}$$

In actual operation, due to the complexity of the system operating environment and the time-varying characteristics of the battery, these factors may lead to the variation of the process noise Q_k and the measurement noise R_k in the system, and thus the estimation accuracy of the algorithm is degraded. Therefore, the idea of adaptive filtering based on the covariance matching principle is introduced in this study.

The specific adaptive noise correction process is expressed in the following Eq. (22):

$$\begin{cases} C_k = \frac{1}{L}\sum_{n=k-L+1}^{k} e_n e_n{}^T \\ Q_k = K_k C_k K_k^T \\ R_k = C_k + C_k P_{\frac{k}{k-1}} C_k^T \end{cases} \tag{22}$$

In Eq. (22), e_n=$y_n - \hat{y}_n$, which is the voltage residual of the battery model at time step n; L is a free parameter that needs to be adaptive.

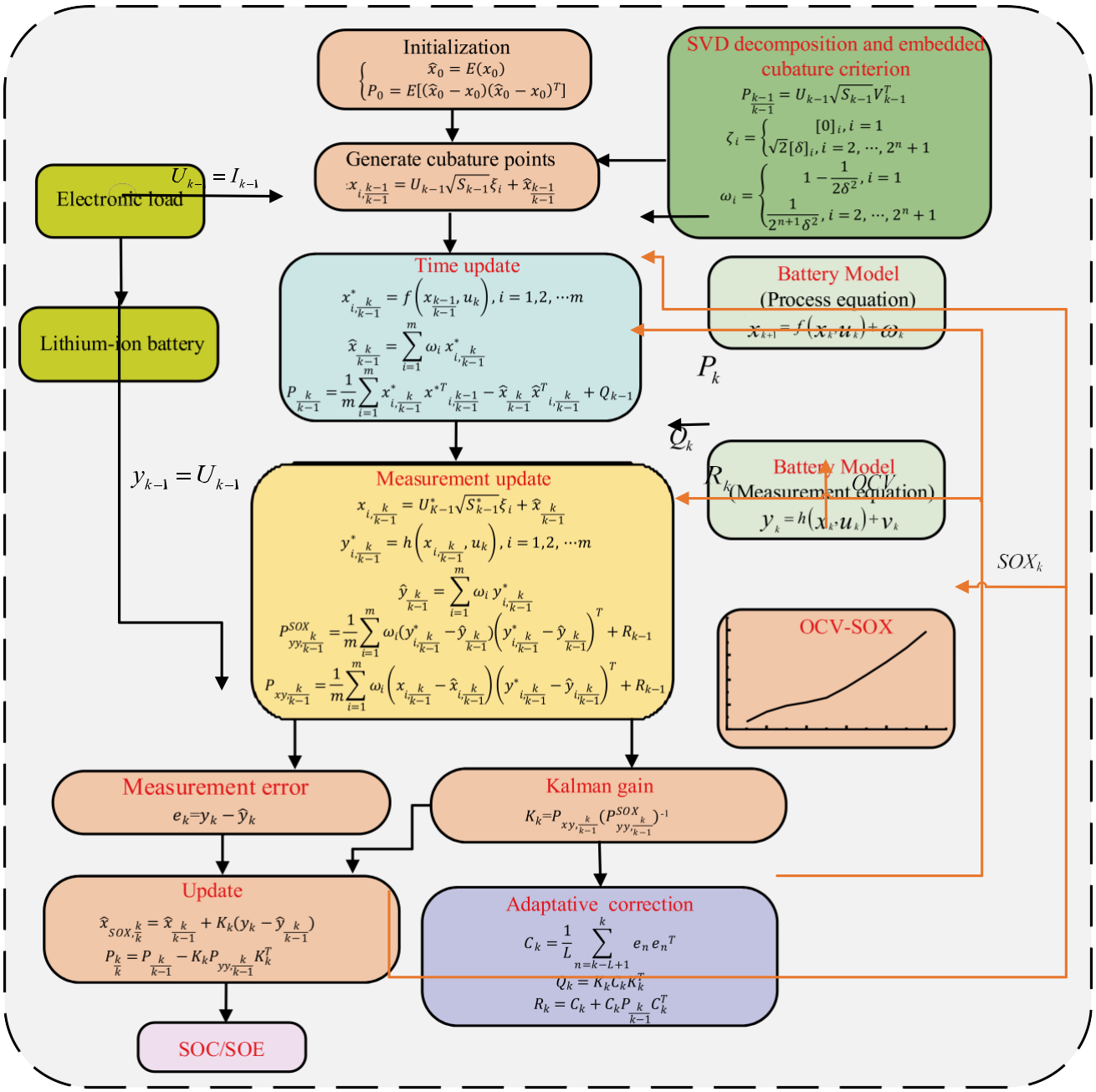

Fig. 3 Flow chart of SOC and SOE joint estimation for the SVD-AECKF algorithm

The covariance of Q_k and R_k in the system is adaptively corrected and updated by using the innovation sequence C_k of the real measured voltage and the model output voltage. An improved singular value decomposition-adaptive embedded cubature Kalman filtering (SVD-(AECKF) algorithm is obtained. This avoids the algorithm filtering accuracy degradation and divergence to ensure the accuracy of battery performance estimation. The flow chart of the SVD-AECKF algorithm for joint SOC and SOE estimation is shown in Fig. 3.

Experimental analysis

In this section, data relating to the current, voltage, and SOC of lithium-ion batteries will be obtained experimentally under complex operating conditions. Model parameter identification and joint estimation validation analysis will also be carried out based on the obtained data. In addition, three evaluation criteria are used for the validation analysis in this article, which are maximum error, root mean square error (RMSE), and mean absolute error (MAE). The mathematical definitions of the above evaluation criteria are as follows.

$$\begin{cases} RMSE = \sqrt{\frac{\sum_k^N (y_{\text{Real}} - y_{\text{Est}})^2}{N}} \\ MAE = \frac{\sum_k^N |y_{\text{Real}} - y_{\text{Est}}|}{N} \end{cases} \tag{23}$$

In Eq. (23), y_{Real} is the real value and y_{Est} is the estimated value. N is the number of experimental data.

Experimental platform

The experiments in this study used 70-Ah power LIBs with a rated voltage of 3.7 V. The BTS200-100–104 battery test equipment was used as the test platform, and software installed in the PC control terminal is used to control the charging and discharging conditions of the battery to match the test equipment. The experimental platform established in this study is shown in Fig. 4.

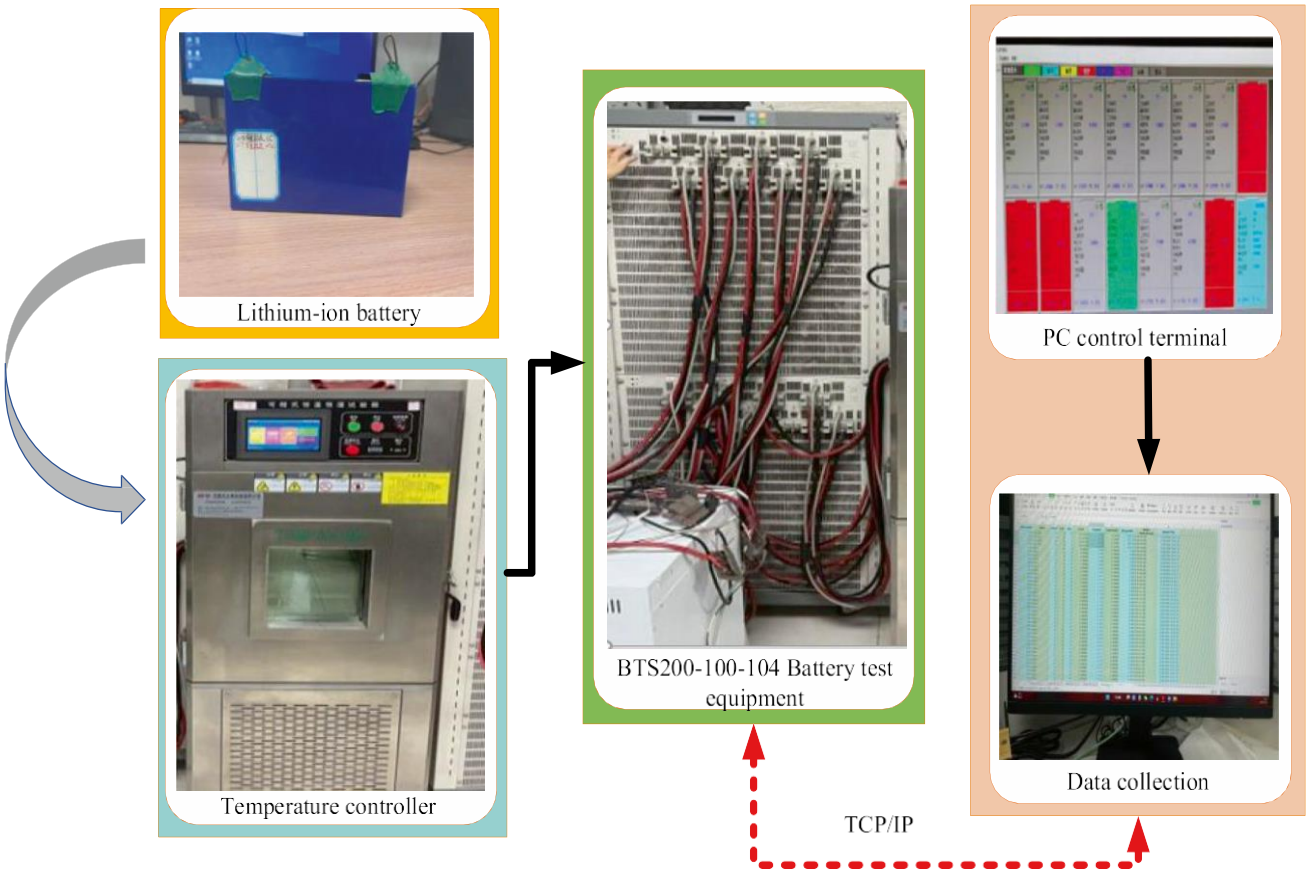

Fig. 4 Schematic diagram of experimental platform construction

Table 1 Comparison of voltage error between the FFRLS and TVFFRLS algorithms

Method	MAE%	RMSE%
TVFFRLS	0.64	0.81
FFRLS	1.04	1.11

Co-estimation results of SOC and SOE

Experimental analysis under HPPC working condition

In practical applications, the complex and variable currents of lithium-ion batteries impose stringent requirements on the dynamic performance of the batteries. To verify the convergence and stability of the online SOC estimation and the accuracy and reliability of the online SOE estimation proposed by the proposed algorithm. The results of different initial error algorithms and actual values are analyzed and verified under the hybrid pulse power characteristic (HPPC) working conditions selected. The experimental results are shown in Figs. 7 and 8.

From Fig. 7(a) and (c), it can be seen that for the initial SOC values of 0.9 and 0.8, the convergence times of the CKF algorithm for SOC estimation are 192 s and 200 s. The convergence times of the ECKF algorithm for SOC estimation are 133 s and 154 s, which are 30.7% and 23.0% faster than the CKF algorithm, respectively. The convergence times of the SVD-ECKF algorithm for SOC estimation are 75 s and 89 s, which are 43.6% and 42.2% faster than the ECKF algorithm, respectively. The convergence times of the SVD-AECKF algorithm for SOC estimation are 36 s and 42 s, which are 44.0% and 52.8% faster than the SVD-ECKF algorithm, respectively. From Fig. 7(b) and (d), it can be seen that when estimating the SOC for different initial values, the valuation of the SOC at the end of discharge shows a large error due to the severe electro- chemical reactions occurring in the battery. The comparative analysis with the other three algorithms reveals that the SVD-AECKF algorithm converges faster and it can converge to the actual more accurately, effectively improving the convergence speed of the filtering algorithm.

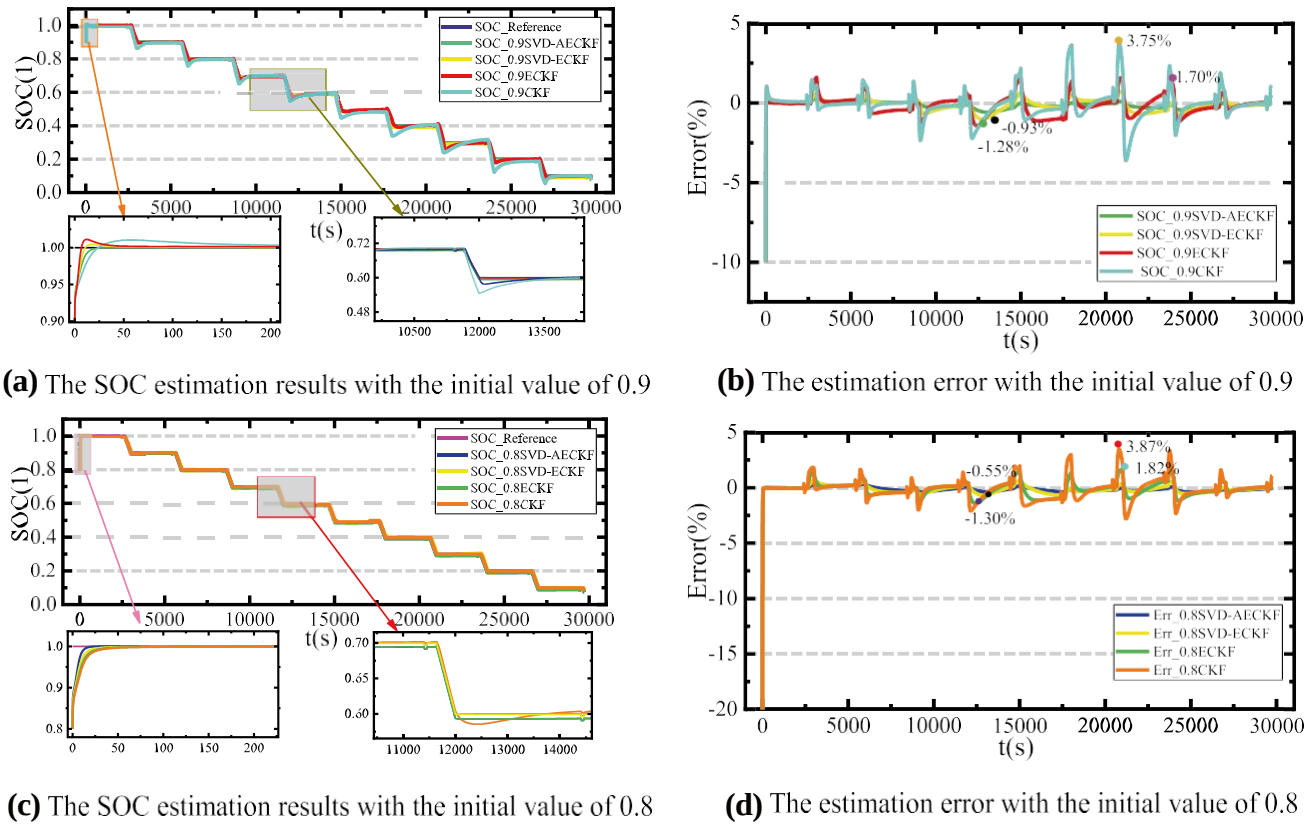

(a) The SOC estimation results with the initial value of 0.9

(b) The estimation error with the initial value of 0.9

(c) The SOC estimation results with the initial value of 0.8

(d) The estimation error with the initial value of 0.8

Fig. 7 Comparison of SOC estimation results for different initial values under HPPC working conditions

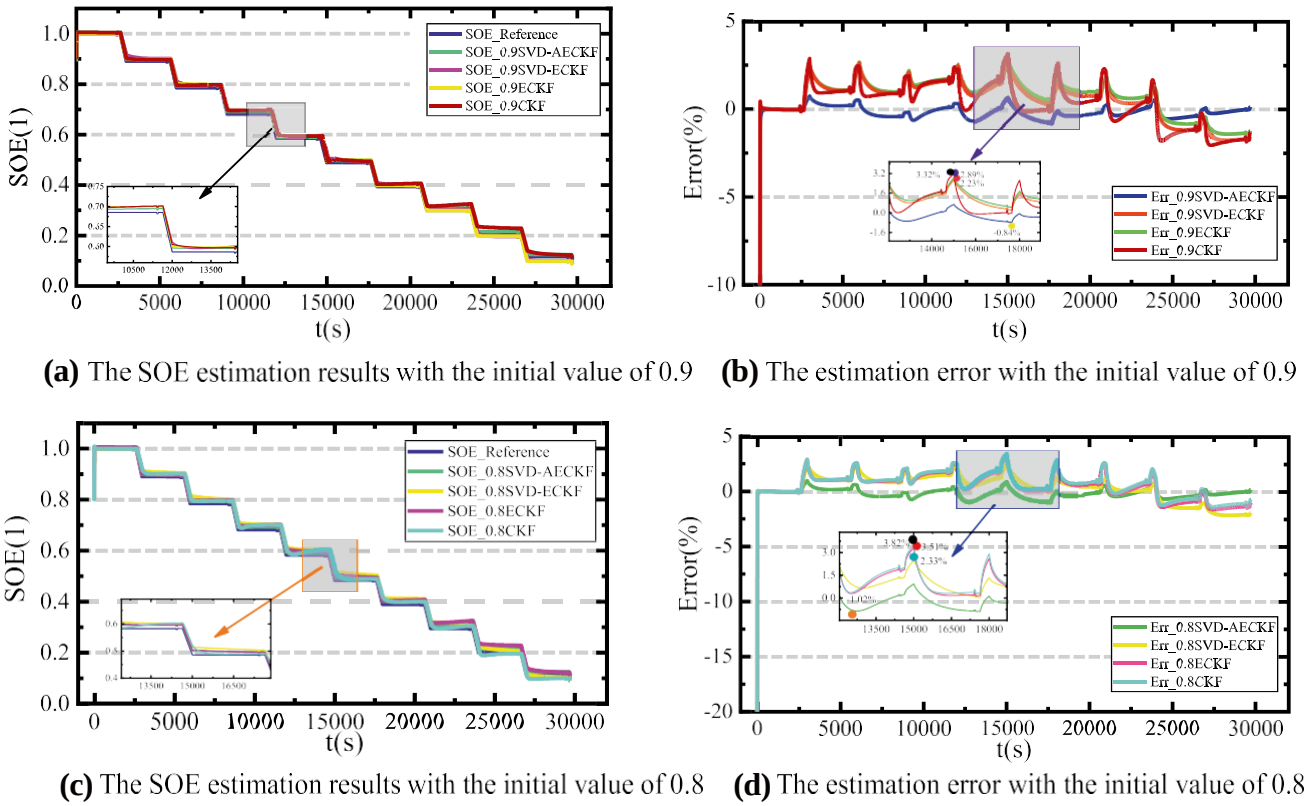

(a) The SOE estimation results with the initial value of 0.9 **(b)** The estimation error with the initial value of 0.9

(c) The SOE estimation results with the initial value of 0.8 **(d)** The estimation error with the initial value of 0.8

Fig. 8 Comparison of SOE estimation results for different initial values under HPPC working conditions

As can be seen from Table 2, the RMSE of the SOE estimation for the SVD-AECKF algorithm is 0.69% and 0.72% for the initial values of SOE of 0.9 and 0.8, respectively. The errors of the other three algorithms are larger than the SVD-ECKF algorithm. The error of the SVD-AECKF algorithm is 35.7% lower than the SVD-ECKF algorithm. By combining convergence time and error, it is shown that the SVD-AECKF algorithm has better estimation accuracy and stability than the other three algorithms under this condition.

Table 2 Comparison of error results of SOC estimation in HPPC working conditions

Method	Initial value	HPPC		
		Convergence time (s)	Maximum error (%)	RMSE (%)
CKF	0.9	192	3.75	3.20
	0.8	200	3.87	3.42
ECKF	0.9	133	1.70	1.31
	0.8	154	1.82	1.48
SVD-ECKF	0.9	75	1.28	1.07
	0.8	89	1.30	1.12
SVD-AECKF	0.9	36	0.93	0.69
	0.8	42	0.98	0.72

As can be seen in Fig. 8(a) and (c), the estimation results of the SVD-AECKF algorithm are very close to the actual values for different initial SOE values. From the enlarged plot in Fig. 8(b), it can be seen that when the initial error of SOE is 10%, the maximum error of SOE estimation of the SVD-AECKF algorithm is 0.84%. Even if the initial error exists, the algorithm can still track and converge stably in time, and the convergence speed is relatively fast. However, the SOE estimation errors of the CKF algorithm, ECKF algorithm, and SVD-ECKF are large, with maximum estimation errors of 3.32%, 2.89%, and 2.23%, respectively. As can be seen from the enlarged plot in Fig. 8(d), when the SOE has an initial error of 20%, the maximum estimation errors of the CKF algorithm, ECKF algorithm, SVD-ECKF algorithm, and SVD-AECKF algorithm are 3.82%, 3.51, 2.33%, and 1.01%, respectively. The comparative analysis reveals that compared with the other three algorithms, the SVD- AECKF algorithm not only effectively reduces the influence of noise on the estimation error and improves the accuracy but also makes the estimation results more stable. This fully proves the accuracy of the algorithm proposed in this paper for estimating SOE.

Table 3 Comparison of error results of SOE estimation with different initial values in HPPC working conditions

Method	Initial value	HPPC	
		Maximum error (%)	RMSE (%)
CKF	0.9	3.32	2.88
	0.8	3.82	3.32
ECKF	0.9	2.89	2.67
	0.8	3.51	3.28
SVD-ECKF	0.9	2.23	2.04
	0.8	2.33	2.12
SVD-AECKF	0.9	0.84	0.65
	0.8	1.02	0.81

As can be seen from Table 3, the RMSE of the SVD- AECKF algorithm for SOE estimation is 0.68% and 0.81% for initial SOE values of 0.9 and 0.8, respectively. With small error fluctuations, the SVD-AECKF algorithm with different initial values of SOE reduces the error by at least 71.8%, 60.2%, and 32.5% compared with the SOE estimation errors of the CKF algorithm, ECKF algorithm, and SVD-ECKF, respectively. It indicates that the proposed algorithm gives more accurate SOE estimation results than the other three algorithms.

Experimental analysis under BBDST working condition

Due to the complex and changeable conditions of the LIBs in the practical application of new energy electric vehicles, to further verify the effectiveness and feasibility of the joint algorithm in the practical application, experiments were carried out under BBDST conditions. BBDST working conditions are derived from the actual data collection of the Beijing bus dynamic test, including the authenticity of various operating data such as starting, taxiing, accelerating, etc., which makes the verification algorithm more convincing. The experimental results of SOC estimation and SOE estimation of the three algorithms under BBDST conditions are shown in Figs. 9 and 10.

The estimation results of the SVD-AECKF algorithm, SVD-ECKF algorithm, ECKF algorithm, and CKF algorithm for different initial SOC values under BBDST conditions are shown in Fig. 9. As can be seen in Fig. 9(a) and (c), the overall SOC estimation shows a fluctuating downward trend due to the alternating charging and discharging during the discharge process. For the initial SOC values of 0.9 and 0.8, the estimated SOC convergence times of the SVD-ECKF algorithm are 25 s and 30 s, respectively, and the convergence speed is at least 26.4% faster than the SVD-ECKF algorithm. The convergence speed of the SVD-ECKF is at least 32.0% faster than the ECKF algorithm. Compared with the CKF algorithm, the ECKF algorithm converges faster. The convergence speed of the ECKF algorithm is at least 16.6% faster than the CKF algorithm. The comparative analysis shows that the SVD-AECKF algorithm performs SOC estimation better than the other three algorithms in terms of filtering stability and convergence speed, and it can converge to close to the true value with higher accuracy and better stability in a short time.

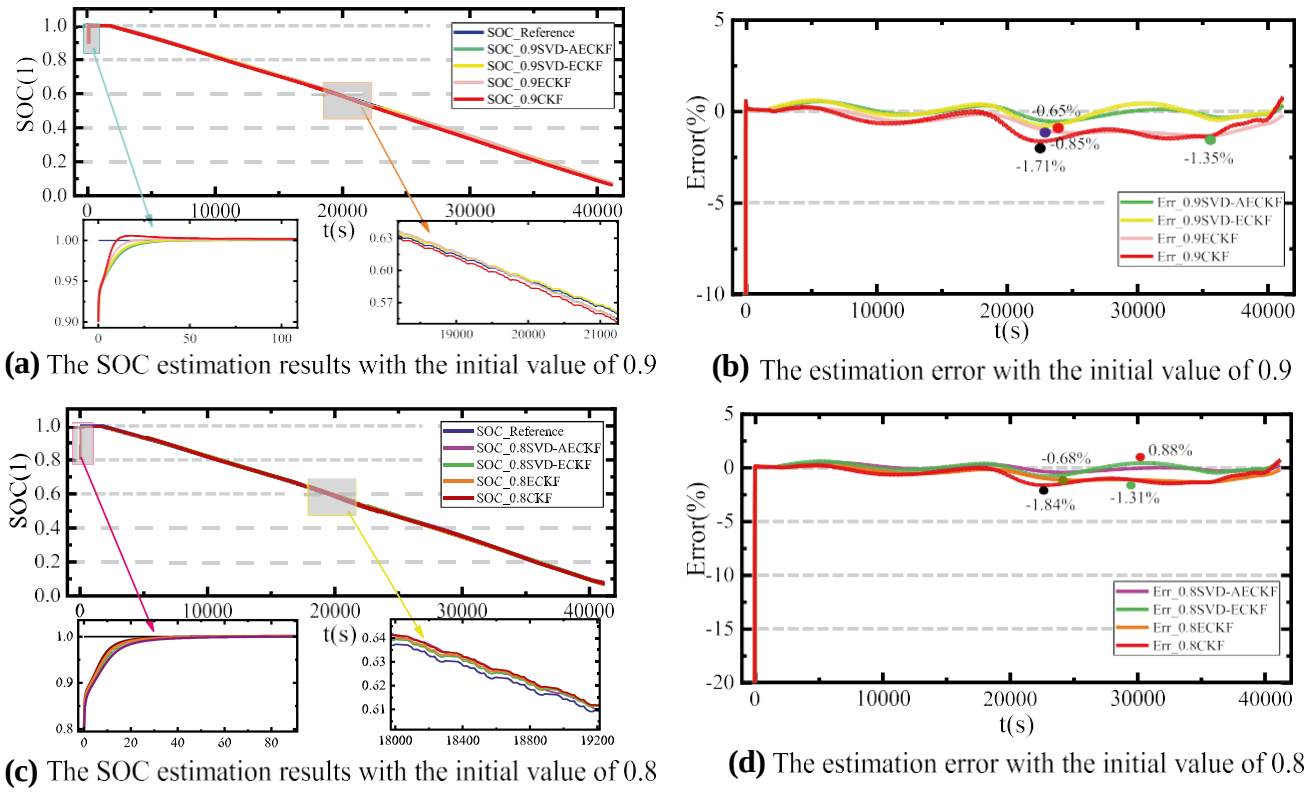

(a) The SOC estimation results with the initial value of 0.9

(b) The estimation error with the initial value of 0.9

(c) The SOC estimation results with the initial value of 0.8

(d) The estimation error with the initial value of 0.8

Fig. 9 Comparison of SOC estimation results for different initial values under BBDST working conditions

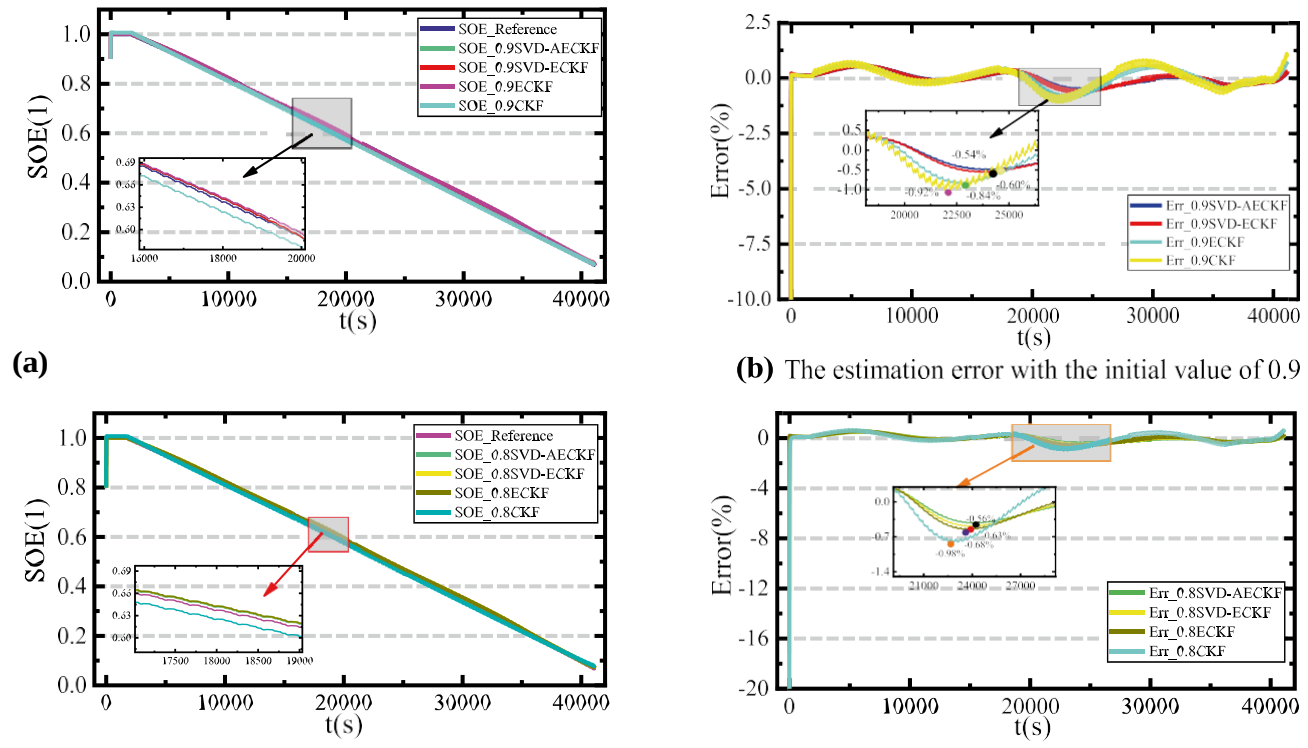

(a)

(b) The estimation error with the initial value of 0.9

(c) The SOE estimation results with the initial value of 0.8

(d) The estimation error with the initial value of 0.8

Fig. 10 Comparison of SOE estimation results for different initial values under BBDST working conditions

Table 4 Comparison of error results of SOC estimation with different initial values in BBDST working conditions

Method	Initial value	BBDST		
		Convergence time (s)	Maximum error (%)	RMSE (%)
CKF	0.9	60	1.71	1.47
	0.8	67	1.84	1.54
ECKF	0.9	50	1.35	1.21
	0.8	56	1.31	1.19
SVD-CKF	0.9	34	0.85	0.71
	0.8	41	0.88	0.76
SVD-AECKF	0.9	25	0.65	0.57
	0.8	30	0.68	0.60

As can be seen from Table 4, the maximum error and RMSE of the SVD-AECKF algorithm with different initial values of SOC are smaller than those of the other three algorithms. When the initial value error of SOC is 10%, the maximum error of SVD-ACKF is 0.65% and the RMSE is 0.57%, which are at least 59.1%, 52.8%, and 22.8% lower than the errors of the CKF algorithm, ECKF algorithm, and SVD-ECKF algorithm, respectively. When the initial value error of SOC is 20%, the maximum error and RMSE of SVD-ACKF are 0.68% and 0.60%, and the errors are smaller than the estimation errors of the CKF algorithm, ECKF algorithm, and SVD-ECKF. Combining the convergence times in Table 4, it can be analyzed that the SOC estimation of the SVD-AECKF algorithm is accurate and effective and has fast convergence speed.

When the initial value of SOE is 0.9, the SOE estimation results of the proposed SVD-AECKF algorithm, SVD-ECKF algorithm, ECKF algorithm, and CKF algorithm are shown in Fig.10(a) and (b). From the enlarged plot in Fig. 10(a), it can be seen that the SOE estimation of the SVD-AECKF algorithm is closer to the actual value and tracks the actual value well to obtain a good estimation accuracy. As shown in Fig. 10(b), the maximum errors of SOE estimation for the SVD-AECKF algorithm, SVD-ECKF algorithm, ECKF algorithm, and CKF algorithm are 0.54%, 0.60%, 0.84%, and 0.92%, respectively.

In addition, Fig.10(c) and (d) shows the SOE estimation results when the initial values are both 0.8. From the enlarged plots, it can be seen that the SOE estimation of the SVD-AECKF algorithm is closer to the reference value with a maximum error of 0.58%. The maximum error of the CKF algorithm is 0.98%. The maximum error of the ECKF algorithm is 0.84%, which is smaller than the CKF algorithm. The error of the SVD-ECKF algorithm is 0.60%, which is smaller than the ECKF algorithm. By comparing the different algorithms, it can be concluded that the SOE estimation error of the SVD-AECKF algorithm is smaller than the other three algorithms, and the SOE estimation is more stable and more accurate.

Table 5 Comparison of error results of SOE estimation with different initial values in BBDST working conditions

Method	Initial value	BBDST	
		Maximum error (%)	RMSE (%)
CKF	0.9	0.92	0.76
	0.8	0.98	0.82
ECKF	0.9	0.84	0.72
	0.8	0.68	0.65
SVD-ECKF	0.9	0.60	0.54
	0.8	0.63	0.58
SVD-AECKF	0.9	0.54	0.47
	0.8	0.58	0.51

As can be seen from Table 5, for initial SOE values of 0.9 and 0.8, the RMSE of the SVD-AECKF algorithm for SOE estimation is 0.47% and 0.51%, respectively. With small error fluctuations, the SVD-AECKF algorithm with different initial values of SOE reduces the error by at least 442.6%, 34.7%, and 12.0% compared with the SOE estimation errors of the CKF algorithm, ECKF algorithm, and SVD-ECKF algorithm, respectively. Combining analysis concludes that the proposed algorithm gives more accurate SOE estimation results than the other three methods. This indicates that the SVD-AECKF algorithm can effectively improve the accuracy of SOE estima- tion for the LIBs.

Conclusion

In this paper, an innovative SVD-AECKF algorithm is proposed to improve the efficiency and accuracy of joint SOC and SOE estimation during complex driving environments for LIBs in new energy vehicles. Through validation and comparative analysis under complex operating conditions, the following conclusions are drawn.

(1) Under the DST working conditions, the parameter identification error of the TVFFRLS algorithm based on the DP equivalent circuit model is controlled to within 1.10%, which is 21% lower than the error of the FFRLS algorithm.

(2) Under complex operating conditions with different estimated initial values, the convergence time of the SVD-AECKF algorithm for SOC estimation is 36 s, which is at least 26.3% faster than the convergence speed of the other three algorithms. The maximum estimation error of SOE is 0.54%, which is at least 12.0% lower than the error of the other three algorithms.

In conclusion, it is proved that the SVD-AECKF algorithm can improve the joint state estimation of lithium-ion batteries and increase the estimation efficiency and accuracy.

This study provides a theoretical basis for providing battery condition monitoring to ensure that drivers can drive the new energy vehicles safely. However, in the actual driving process, the temperature is complex and variable, and future research directions will focus on considering the impact of real-time temperature changes in the battery state estimation.

Acknowledgements This work is supported by the National Natural Science Foundation of China (No. 62173281), Sichuan Provincial Science and Technology Program (No. 23ZDYF0734NSFSC4444), Dazhou City School Partnership Program (No. DZXQHZ006), Technology Pole Talent Summit Program (No. KJCRCFH08), and Robert Gordon University.

References

1. Qays MO, Buswig Y, Hossain ML, Abu-Siada A (2020) Recent progress and future trends on state of charge estimation methods to improve battery-storage efficiency: a review. CSEE J Power Energy Syst 8(1):105–114
2. Chen H-C et al (2021) Design of a modular battery management system for electric motorcycle. Energies 14(12)
3. Habib AKMA et al (2023) Lithium-Ion battery management system for electric vehicles: constraints, challenges, and recommendations. Batteries 9(3)
4. Hossain Lipu MS et al (2021) Intelligent algorithms and control strategies for battery management system in electric vehicles: progress, challenges and future outlook. J Cleaner Prod 292
5. Li S et al (2022) Edge computing for vehicle battery management: cloud-based online state estimation. J Energy Storage 55
6. Yu X et al (2023) Research on outdoor mobile music speaker battery management algorithm based on dynamic redundancy. Technologies 11(2)
7. Tsai C-T and F-W Peng (2023) Design and implementation of charging and discharging management system for two-set lithium ferrous phosphate batteries. Sens Mater 35(4)
8. Li Z, Xu W, Hu X (2013) Research on the development of new energy vehicle industry in China. Appl Mech Mater 291–294:861–865
9. Xia B et al (2022) Verification platform of SOC estimation algorithm for lithium-ion batteries of electric vehicles. Energies 15(9)
10. Yuan X, Liu X, Zuo J (2015) The development of new energy vehicles for a sustainable future: a review. Renew Sustain Energy Rev 42:298–305
11. Zheng L et al (2022) Tracing of lithium supply and demand bottleneck in China's new energy vehicle industry—based on the chart of lithium flow. Front Energy Res 10
12. Li Y, Yang J, Song J (2017) Design principles and energy system scale analysis technologies of new lithium-ion and aluminum-ion batteries for sustainable energy electric vehicles. Renew Sustain Energy Rev 71:645–651
13. Li H et al (2022) Industrial policy and technological innovation of new energy vehicle industry in China. Energies 15(24)
14. Hongwen H et al (2011) State-of-charge estimation of the lithium-ion battery using an adaptive extended Kalman filter based on an improved Thevenin model. IEEE Trans Veh Technol 60(4):1461–1469

15. Li X, Wang Z, Zhang L (2019) Co-estimation of capacity and state-of-charge for lithium-ion batteries in electric vehicles. Energy 174:33–44
16. Espedal IB et al (2021) Current trends for state-of-charge (SoC) estimation in lithium-ion battery electric vehicles. Energies 14(11)
17. Yun L et al (2018) Experimental combined numerical approach for evaluation of battery capacity based on the initial applied stress, the real-time stress, charging open circuit voltage, and discharging open circuit voltage. Math Probl Eng 2018:1–16
18. Zhang M et al (2023) A review of SOH prediction of Li-ion batteries based on data-driven algorithms. Energies 16(7)
19. Mao X, Song S, Ding F (2022) Optimal BP neural network algorithm for state of charge estimation of lithium-ion battery using PSO with Levy flight. J Energy Storage 49
20. Kwak M (2022) A variable-length scale parameter dependent state of charge estimation of lithium ion batteries by Kalman filters. Int J Electrochem Sci
21. Yang S et al (2021) A parameter adaptive method for state of charge estimation of lithium-ion batteries with an improved extended Kalman filter. Sci Rep 11(1):5805
22. Zhang Z-L et al (2017) SOC estimation of lithium-ion batteries with AEKF and wavelet transform matrix. IEEE Trans Power Electron 32(10):7626–7634
23. Zhu Q et al (2019) A state of charge estimation method for lithium-ion batteries based on fractional order adaptive extended kalman filter. Energy 187
24. Chen Z et al (2016) A novel state of charge estimation algorithm for lithium-ion battery packs of electric vehicles. Energies 9(9)
25. Sun D et al (2021) State of charge estimation for lithium-ion battery based on an intelligent adaptive extended Kalman filter with improved noise estimator. Energy 214
26. Wang C et al (2022) A novel ultracapacitor state-of-charge fusion estimation method for electric vehicles considering temperature uncertainty. Energies 15(12)
27. Zhuang S et al (2022) Research on estimation of state of charge of Li-ion battery based on cubature Kalman filter. J Electrochem Soc 169(10)
28. Ning Z et al (2022) Co-estimation of state of charge and state of health for 48 V battery system based on cubature Kalman filter and H-infinity. J Energy Storage 56
29. Song Q (2021) A novel joint support vector machine-cubature Kalman filtering method for adaptive state of charge prediction of lithium-ion batteries. Int J Electrochem Sci
30. Xing L et al (2022) Lithium battery SOC estimation based on multi-innovation unscented and fractional order square root cubature Kalman filter. Appl Sci 12(19)
31. Zeng Z et al (2018) An online state of charge estimation algorithm for lithium-ion batteries using an improved adaptive cubature Kalman filter. Energies 11(1)
32. Zhang K et al (2019) State of charge estimation for lithium battery based on adaptively weighting cubature particle filter. IEEE Access 7:166657–166666
33. An F et al (2022) State of energy estimation for lithium-ion battery pack via prediction in electric vehicle applications. IEEE Trans Veh Technol 71(1):184–195
34. Lai X et al (2021) A novel method for state of energy estimation of lithium-ion batteries using particle filter and extended Kalman filter. J Energy Storage 43
35. Mei P et al (2022) A learning-based vehicle-cloud collaboration approach for joint estimation of state-of-energy and state-of- health. Sensors (Basel) 22(23)
36. Naseri F et al (2020) Online parameter estimation for supercapaci- tor state-of-energy and state-of-health determination in vehicular applications. IEEE Trans Industr Electron 67(9):7963–7972
37. Fan T-E et al (2022) Simultaneously estimating two battery states by combining a long short-term memory network with an adaptive unscented Kalman filter. J Energy Storage 50
38. Ma L, Hu C, Cheng F (2021) State of charge and state of energy estimation for lithium-ion batteries based on a long short-term memory neural network. J Energy Storage 37
39. Shrivastava P et al (2021) Combined state of charge and state of energy estimation of lithium-ion battery using dual forgetting factor-based adaptive extended Kalman filter for electric vehicle applications. IEEE Trans Veh Technol 70(2):1200–1215
40. Shrivastava P et al (2022) Comprehensive co-estimation of lithium-ion battery state of charge, state of energy, state of power, maximum available capacity, and maximum available energy. J Energy Storage 56
41. Zhang S, Zhang X (2022) A novel non-experiment-based recon- struction method for the relationship between open-circuit-voltage and state-of-charge/state-of-energy of lithium-ion battery. Elec- trochimica Acta 403
42. Xia L (2021) A novel prior noise correction - adaptive extended Kalman filtering method for the full parameter and state-of-energy co-estimation of the Lithium-ion Batteries. Int J Electrochem Sci
43. Xu W et al (2019) A multi-timescale estimator for lithium-ion battery state of charge and state of energy estimation using dual H infinity filter. IEEE Access 7:181229–181241
44. Yang X et al (2022) A novel fuzzy adaptive cubature Kalman filtering method for the state of charge and state of energy co-estimation of lithium-ion batteries. Electrochimica Acta 415
45. Zhang S, Peng N, Zhang X (2021) An application-oriented multi- state estimation framework of lithium-ion battery used in electric vehicles. Int J Energy Res 45(13):18554–18576